WAVES IN RANDOM AND COMPLEX MEDIA

https://www.tandfonline.com/journals/twrm20

Impact factor = 4.853

ACCEPTED MAY 2ND 2023

Numerical Study of Transient Convective Turbulent Boundary Layer Flow along a Vertical Plate: Analysis of Kinetic Energy and its Dissipation rate

S.P. Suresha[1], G Janardhana Reddy[1,*], Mahesh Kumar[2], H. P. Rani[3] and O. Anwar Bég[4]

[1]*Laboratory on Computational Fluid Dynamics, Department of Mathematics, Central University of Karnataka, Kalaburagi-585367, India.*

[2]*Department of Applied Mathematics and Humanities, Sardar Vallabhai National Institute of Technology, Surat, Gujarat-395007, India.*

[3]*Department of Mathematics, National Institute of Technology, Warangal-506004, India.*

[4]*Professor, Multi-physical Engineering Sciences, Aeronautical/ Mechanical Engineering Department, School of Science, Engineering and Environment, Salford University, Manchester M54WT, UK.*

*Corresponding author: gjr.nitw@gmail.com

Abstract:

The present article numerically investigates the turbulent buoyancy-driven (natural convection) flow along a vertical plate with a low Reynolds turbulence two-equation *k*-ε model. The deployed turbulence model is appropriate for low Reynolds number (LRN) turbulent flow adjacent to a solid boundary, and the turbulence kinetic energy (TKE) and dissipation rate of TKE are estimated using the momentum equations and are solved simultaneously with the mean flow conservation equations. Two-dimensional time-dependent viscous incompressible turbulent flow is simulated. This flow domain is governed by a highly non-linear group of partial differential equations, namely the time-averaged continuity, momentum, and energy, and also the flow property ν_t is determined through TKE, and dissipation rate of TKE equations. Since these equations are not solvable using analytical methods, an implicit second order finite difference method is employed to solve the governing turbulent flow equations numerically. The simulated time-averaged velocity, temperature, TKE, and dissipation rate of TKE profiles along with friction factor and heat transfer rate are computed for different values of turbulent Reynolds (Re) and Prandtl (Pr) numbers. Average velocity, temperature, turbulence energy, and dissipation rate under both transient and steady state conditions are decreased with increment in Pr. There is a decrement in average transient velocity and

turbulence energy rates with increasing Re values, whereas the average temperature profile increases. Average steady temperature and turbulence energy profiles are also enhanced with rising values of Re. The majority of researchers focus on laminar flow and thusfar turbulent flow has mainly been addressed through experiments only. To better elucidate the flow in this condition, *the novelty of the present study is to utilize a numerical FDM procedure to probe more deeply into the turbulence characteristics in buoyancy-driven (natural convection) flow along a vertical plate with a low Reynolds turbulence two-equation k-ε model, as this topic is fundamental to many applications in science and engineering*. Furthermore, the results of the turbulent flow simulations obtained from the current model are corroborated with existing results for the special case of laminar flow and a good correlation is achieved.

Keywords: *Turbulent flow, vertical plate, k-ε model, low Reynolds number (LRN), natural convection; implicit second order finite difference method.*

Nomenclature:

x : Vertical coordinate in the path of average flow

y : Horizontal coordinate normal to the plate

X : Dimensionless axial coordinate in the path of average flow

Y: Dimensionless horizontal coordinate normal to the plate

u, v : Velocities along x and y directions respectively

$\bar{u}$, $\bar{v}$: Time average velocities along x and y directions respectively

u', v' : Fluctuating velocities along x and y directions respectively

$\overline{u'v'}$: Turbulent shear stress

$\overline{u'T'}$: Longitudinal turbulent heat flux

τ_w : Total wall shear stress

U, V : Dimensionless velocities along x and y directions respectively

θ : Temperature field

$\bar{T}$: Time-averaged temperature

T': Fluctuating temperature

T : Dimensionless temperature

t' : Time

t : Non-dimensional time

g : Gravitational field

Gr : Thermal Grashof parameter

Pr : Turbulent Prandtl number

C_1, C_2 : Empirical constants

C_k: Arbitrary Prandtl number-dependent coefficient

f_1, f_2, f_μ : Damping functions

k : Time average turbulence energy

ϵ : Time average turbulence energy dissipation rate

K : Dimensionless turbulence energy

E : Dimensionless turbulence energy dissipation rate

Re : Turbulent Reynolds number

C_k : Arbitrary Prandtl number dependent coefficient.

C_μ : Proportional constant

K_T : Thermal conductivity

$\bar{u}_\infty$: Free stream velocity

$\beta_{\bar{T}}$: Volumetric thermal expansion coefficient

A : Sub-diagonal entries of the tridiagonal matrix

B : Main diagonal entries of the tridiagonal matrix

C : Super diagonal entries of the tridiagonal matrix

D : Right-hand side matrix in Eq. (30)

Greek symbols:

α_t: Turbulent heat diffusivity

σ_T, σ_k : Turbulent Prandtl numbers for $\bar{T}$and k

σ_ϵ : Dissipation Prandtl number

μ : Dynamic viscosity

μ_t : Dynamic viscosity for turbulent flow

ν, ν_t : Laminar and turbulent kinematic viscosities respectively

ρ : Density

Subscripts:

l, m : (X, Y) coordinate grid levels

w: Surface condition

∞: Free stream condition

Superscripts:

n: Time step level

1. Introduction:

Natural convection often known as "*buoyancy-driven flow*" is an important phenomenon in thermo-fluid dynamics. Density differences due to temperature gradients within the fluid flow mobilize free convection currents. Laminar and turbulent flows are present in many of the motions in nature and industry. In particular aspects of solar and stellar dynamics, geophysics of the earth's mantle, atmospheric flows, transport engineering (aircraft, naval, automotive), marine hydrodynamics, and other scientific fields all exhibit turbulent natural convection flows in various ways. Depending on the fluid under discussion and the geometrical parameters of the arrangement under study, natural convection flows can either be laminar or turbulent. Contrary to laminar flow, turbulent flow is characterized by changes in flow properties. With high transport momentum, energy, and mass of the turbulence, the flow becomes unpredictable, diffusive and dissipative. Mostly, laminar natural convection flow fields have been studied widely in the literature due to their simplicity in comparison with turbulent convective motions. The turbulent motion abundantly noticed in natural phenomena creates more complicated problems due to its complexity involved in solving mathematical equations. These turbulent flows have been investigated since the early twentieth century. Such flows find applications in the thermal energy storage systems, heat exchangers, propulsion duct near wall flows, electronic cabin cooling, thermal behavior in turbine nacelles [1], inverse buoyancy-driven heat transfer problems [2], heat transfer in rectangular geometries [3] and interaction of energy transfer in industrial metallurgical processes involving open channels [4] among many other technological systems.

Transient buoyancy-driven flow along a heated vertical geometry is one of the primary areas of interest for examining the fundamentals of turbulence with heat transfer. Many researchers focused on the study of the natural convection turbulent flow concept in the1970s and many experimental works [5-7] were conducted. Launder and Jones [8-9] presented an improved theoretical study for turbulent convective flow adjacent to the vertical plate. They considered the two-equation k-ε turbulence model and predicted the reverse-transition turbulence using low Reynolds number phenomena. Subsequently, many other theoretical and

computational studies were communicated [10-20] which have addressed a variety of configurations including vertical heated walls, channels, enclosures, and wall jets. More recently Rath and Dash [21] reported a computational study of buoyancy-driven turbulent flow from a horizontal cylinder in a 3-dimensional domain. They have conducted numerical simulations for both turbulent and laminar regimes for different values of Rayleigh number and also developed a novel correlation of heat transport rate, which would be advantageous for industrial practitioners. Further, Acharya and Dash [22] investigated numerically the natural convection in turbulent flow from a hollow cylinder and solved the governing flow-field equations over a selected range of Rayleigh numbers.

The above-mentioned studies are applicable to *steady* flows; however, in the vast majority of engineering problems, *time-dependent* flows occur. Unsteady flows arise in both external flows (e.g., helicopter rotor blades, coating dynamics) and internal flows (e.g., on turbomachinery blades, blade flutter prediction, and prevention, materials processing, etc). In such flow regimes, unsteadiness contributes strongly to the transition from laminar flow to turbulent flow, separated and vortical flows, etc. In view of these applications, several investigators have considered the unsteady turbulent boundary layer flow for different flow configurations [23-25]. Fan *et al.* [26] analyzed the transient turbulent flow in a near wall region using the improved low Reynolds number (LRN) k-ε model. They showed that the improved turbulence model (k-ε) is more accurate for the assessment of near wall regions in comparison to other turbulent models, such as k-ω, Spalart-Allmaras, Reynolds' stress equation model (RSM), Mentor's shear stress transport (SST) model, etc. Abe *et al.* [27] studied the time-dependent turbulent heat transfer in separating flows deploying also the LRN model with the Kolmogorov velocity scale. Bredberg and Davidson [28] presented a novel LRN model for the channel geometry and included transient results for fully developed flow. Bentaleb *et al.* [29] investigated numerically the transient turbulent flow in a channel and compared their computational results with experimental data. Further, Nie and Li [30] investigated the LRN model (k-ε) by modifying the fundamental k-ε turbulence model. They have shown that the proposed model applies to the entire fluid region and is more accurate than other turbulence models. Recently, Behara and Rathore [31] used the LRN turbulence model to simulate the 2-dimensional turbulence wall jet flow from a moving plate with a finite volume scheme. Wen *et al.* [32] studied the transition from laminar flow to turbulent flow within the boundary layer adjacent to an isothermal wall in a cubical cavity. Further, recent research work related to LRN can be observed in the literature [33-36].

From the above discussions and literature survey, it can be concluded that the majority of natural convection studies have been limited to the laminar regime. Also, studies on turbulent natural convection flows have been confined to the *steady-state* region using different computational schemes and turbulence models. However, very few articles have addressed turbulent natural convection flows under transient conditions. Further, the experimental approach to resolve these complicated problems is costly and time consuming. Numerical methods are less expensive and have comparatively large flexibility for accommodating complex geometrical systems and boundary conditions. Motivated by significant applications of turbulent unsteady convection in engineering sciences, in the present article, we extend the earlier study of Lin and Churchill [12] from steady state to transient to examine turbulent "*free convection flow past a vertical plate using the LRN k-ε turbulence model"*. The time-averaged governing coupled equations are formulated and solved using the Crank-Nicolson second order implicit finite difference method. The obtained numerical results are visualized graphically and analyzed in terms of velocity, temperature, kinetic energy, dissipation rate, momentum, and heat transfer rates.

2. Mathematical model of the turbulent flow:

Time-dependent free convective turbulent boundary layer flow along a stationary vertical plate is considered, as portrayed in **Fig. 1**. A geometry of rectangular shape is considered to describe the 2-dimensional plate flow domain in which the x-axis is measured along the vertical direction and the y-coordinate is normal to the plate. At the initial time $t' = 0$, the ambient average energy field($\bar{T}_\infty$) and the wall temperature ($\bar{T}_w$) of the plate are the same. As time starts, i.e. $t' > 0$, the average thermal field of the plate is increased to $\bar{T}_w (> \bar{T}_\infty)$ and this difference preserved for all $t' > 0$. Therefore, as a result of temperature variations across the boundary layer near the plate, density changes occur and it interacts with the gravity field, then creates the turbulent convection flow over the vertical plate. The resulting family of two-dimensional nonlinear time-averaged Navier-Stokes equations for the mass, momentum, and temperature is described according to the fluid flow and geometry using the Boussinesq approximation. With these assumptions, the governing "*Reynolds averaged Navier-Stokes equations for turbulent flow"* can be expressed as follows [12]:

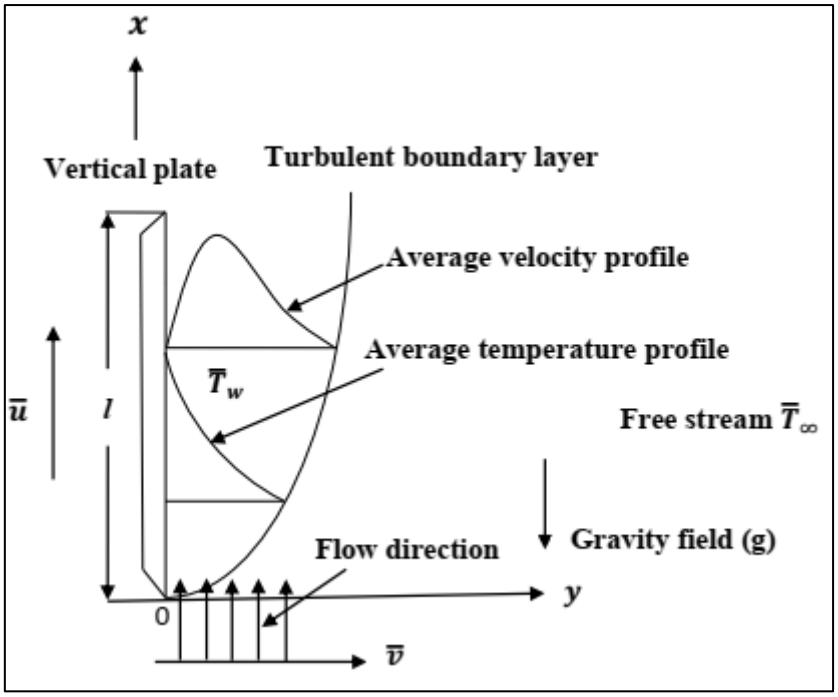

Figure 1: Turbulent convective flow on a vertical plate.

2.1 Governing equations:

$$\frac{\partial \bar{u}}{\partial x} + \frac{\partial \bar{v}}{\partial y} = 0 \tag{1}$$

$$\frac{\partial \bar{u}}{\partial t'} + \frac{\partial}{\partial x}(\bar{u}\bar{u}) + \frac{\partial}{\partial y}(\bar{v}\bar{u}) = g\beta(\bar{T} - \bar{T}_\infty) + \nu\frac{\partial^2 \bar{u}}{\partial y^2} - \frac{\partial}{\partial y}(\overline{u'v'}) \tag{2}$$

$$\frac{\partial \bar{T}}{\partial t'} + \frac{\partial}{\partial x}(\bar{u}\bar{T}) + \frac{\partial}{\partial y}(\bar{v}\bar{T}) = \alpha\frac{\partial^2 \bar{T}}{\partial y^2} - \frac{\partial}{\partial y}(\overline{v'T'}) \tag{3}$$

The instantaneous fluid flow property $(\emptyset)$ is decomposed as a sum of time average and fluctuating components, i.e. $\emptyset = \overline{\emptyset} + \emptyset'$. Here the symbol $\emptyset$ denotes u, v, & θ $\overline{\emptyset}$ indicates $\bar{u}$, $\bar{v}$ & $\bar{T}$, and $\emptyset'$ indicates u', v'& T'.

To simplify the above equations (1)-(3), the Reynolds stress term $\overline{u'v'}$ and fluctuating temperature $(\overline{v'T'})$ are given below as follows[12].

$$\overline{u_i'u_j'} = \frac{2}{3}k\delta_{ij} - \nu_t\left(\frac{\partial \overline{u_i}}{\partial x_j} + \frac{\partial \overline{u_j}}{\partial x_i}\right) \tag{4}$$

In Eq. (4), the term ν_t refers to turbulent kinematic viscosity which is not a fluid property but is highly influenced by the turbulence state. As a result, ν_t will differ significantly from one point of the flow to the next. Also, δ_{ij} is the Kronecker delta function (is one for $i = j$ and zero

for $i \neq j$), and k is the time mean turbulence kinetic energy which is defined as $k \equiv \frac{1}{2}\left(\overline{(u')^2 + (v')^2}\right)$.

For fluctuating temperature, the corresponding model is given by:

$$\overline{u_j' T'} = -\frac{\nu_t}{\sigma_T}\frac{\partial \bar{T}}{\partial x_j} \tag{5}$$

By incorporating the above Reynolds stress term (Eq. (4)) and fluctuating temperature (Eq. (5)) models into the governing Eqs. (1)-(3), the reduced governing equations can be written as follows:

$$\frac{\partial \bar{u}}{\partial x} + \frac{\partial \bar{v}}{\partial y} = 0 \tag{6}$$

$$\frac{\partial \bar{u}}{\partial t'} + \frac{\partial}{\partial x}(\bar{u}\bar{u}) + \frac{\partial}{\partial y}(\bar{v}\bar{u}) = g\beta(\bar{T} - \bar{T}_\infty) + (\nu + \nu_t)\frac{\partial^2 \bar{u}}{\partial y^2} \tag{7}$$

$$\frac{\partial \bar{T}}{\partial t'} + \frac{\partial}{\partial x}(\bar{u}\bar{T}) + \frac{\partial}{\partial y}(\bar{v}\bar{T}) = \left(\alpha + \frac{\nu_t}{\sigma_T}\right)\frac{\partial^2 \bar{T}}{\partial y^2} \tag{8}$$

The following are the initial and boundary conditions that represent the turbulent flow for the considered rectangular plate geometry.

$$\begin{aligned} &t' \leq 0 \text{ and } \forall\, x \,\&\, y; && \bar{u} = 0,\ \bar{v} = 0,\ \bar{T} = \bar{T}_\infty \\ &t' > 0 \text{ and at } y = 0; && \bar{u} = 0,\ \bar{v} = 0,\ \bar{T} = \bar{T}_w \\ &\text{at } x = 0; && \bar{u} = 0,\ \bar{v} = 0,\ \bar{T} = \bar{T}_\infty \\ &\text{as } y \to \infty; && \bar{u} \to 0,\ \bar{v} \to 0,\ \bar{T} \to \bar{T}_\infty \end{aligned} \tag{9}$$

2.1 Turbulence k-ε model:

A two-equation model has been utilized to determine a robust numerical solution for natural convective turbulent flows along the isothermal vertical plate. The k-ε model is used to characterize turbulence flow in this study by computing turbulent viscosity (ν_t) at each location in the flow using the kinetic energy and dissipation rate. Regarding this, Launder and Jones [8] established a model for determining local values of k and ν_t in a general turbulent velocity region without depending on the boundaries. Further, the various empirical coefficients involved in the two-equation model of turbulence are not guaranteed to be applicable to natural convection. However, the k-ε turbulence model has been successfully used to calculate

turbulent *forced convection* and has been shown to be applicable to *free convection (buoyancy-driven)* flow also [8]. For the turbulent kinematic viscosity ν_t, the following term is proposed in this *k*-ε model which is proportional to the velocity scale $k^{1/2}$ and the length scale $\frac{k^{3/2}}{\epsilon}$, that is:

$$\nu_t = C_\mu \frac{k^2}{\epsilon} \tag{10}$$

In Eq. (10), C_μ is an empirical constant. Also, ϵ is the time average dissipation rate of kinetic turbulent energy, which is defined as:

$$\epsilon \equiv \nu \overline{\frac{\partial u'}{\partial y}\frac{\partial u'}{\partial y}} \tag{11}$$

Using the Reynolds decomposition method, the transport equations for kinetic turbulent energy (k) and dissipation rate (ϵ) can be derived from the N-S (Navier-Stokes) equations [43]. Accordingly, after Reynolds decomposition of the momentum equations, multiplying the corresponding fluctuating velocities, then taking the time average of the entire equation and introducing some of the following models [12], the equation for k can be obtained. The emerging relationship is as follows:

$$\overline{u_j'\left(\frac{1}{2}u_i'u_i'\right)} = -\frac{\nu_t}{\sigma_k}\frac{\partial k}{\partial x_j} \tag{12}$$

Also, using Eqs. (4), (11), and (12) along with buoyancy term $g\beta\overline{u'T'}$, the equation of k can be written as:

$$\frac{\partial k}{\partial t'} + \frac{\partial}{\partial x}(\bar{u}k) + \frac{\partial}{\partial y}(\bar{v}k) = \left(\nu + \frac{\nu_t}{\sigma_k}\right)\frac{\partial^2 k}{\partial y^2} + \nu_t\left(\frac{\partial \bar{u}}{\partial y}\right)^2 - \epsilon - C_k g\beta\frac{\nu_t}{\sigma_T}\frac{\partial \bar{T}}{\partial y} \tag{13}$$

Here, in the present study, the considered buoyant production of k is assumed to be negligible i. e. $C_k = 0$ in Eq. (13) which is explained in [12]. Further, the equation for ϵ is also derived from the *time average* of the momentum equation with Reynolds' decomposition. Because of this, the time average of the entire momentum equation is considered, by summing and introducing some models [12] as follows:

$$\overline{u_j'\nu\frac{\partial u_i'}{\partial x_j}\frac{\partial u_i'}{\partial x_j}} = -\frac{\nu_t}{\sigma_\epsilon}\frac{\partial \epsilon}{\partial x_j} \tag{14}$$

$$2\nu\left(\overline{\frac{\partial u_\iota'}{\partial x_k}\frac{\partial u_\iota'}{\partial x_k}}+\overline{\frac{\partial u_k'}{\partial x_\iota}\frac{\partial u_k'}{\partial x_\iota}}\right)=c_1\frac{\epsilon}{k}\overline{u_\iota' u_J'} \tag{15}$$

$$2\left[\nu\overline{\frac{\partial u_\iota'}{\partial x_J}\frac{\partial u_\iota'}{\partial x_k}\frac{\partial u_J'}{\partial x_k}}+\overline{\left(\nu\frac{\partial^2 u_\iota'}{\partial x_J \partial x_k}\right)^2}\right]=c_2\frac{\epsilon^2}{k} \tag{16}$$

$$g\beta\nu\overline{\frac{\partial u_J'}{\partial x_k}\frac{\partial T'}{\partial x_k}}\cong 0 \tag{17}$$

Also, using the above Eqs. (14)-(17) and with the help of Eq. (4), the equation of ϵ can be written as [43]:

$$\frac{\partial\epsilon}{\partial t'}+\frac{\partial}{\partial x}(\bar{u}\epsilon)+\frac{\partial}{\partial y}(\bar{v}\epsilon)=\left(\nu+\frac{\nu_t}{\sigma_\epsilon}\right)\frac{\partial^2\epsilon}{\partial y^2}+C_1\frac{\epsilon\nu_t}{k}\left(\frac{\partial\bar{u}}{\partial y}\right)^2-C_2\frac{\epsilon^2}{k} \tag{18}$$

After deriving the equations for k and ϵ, the corresponding initial and boundary conditions for the Eqs. (13) and (18) together with Eqs. (6)-(8) can be written as follows:

$$\begin{aligned}
&t' \le 0 \text{ and } \forall\, x \,\&\, y; \quad \bar{u}=0,\ \bar{v}=0,\ k=0,\ \epsilon=0,\ \bar{T}=\bar{T}_\infty\\
&t' > 0 \text{ and at } y=0; \quad \bar{u}=0,\ \bar{v}=0,\ k=0,\ \epsilon=0,\ \bar{T}=\bar{T}_w\\
&\text{at } x=0; \quad \bar{u}=0,\ \bar{v}=0,\ k=0,\ \epsilon=0,\ \bar{T}=\bar{T}_\infty\\
&\text{as } y\to\infty; \quad \bar{u}\to 0,\ \bar{v}\to 0,\ k\to 0,\ \epsilon\to 0,\ \bar{T}\to\bar{T}_\infty
\end{aligned} \tag{19}$$

The above model is suitable only for large values of turbulence Reynolds number which is defined as:

$$Re=\frac{k^2}{\nu\epsilon} \tag{20}$$

However, certain adjustments are required if the above model holds true near the wall when Re is of small value.

2.2 Generalisation of the k-ε model for near-wall treatment:

The low Reynolds number (LRN) turbulence model aids in understanding the physics near the wall for *time-dependent wall-bounded average flows*. The LRN is distinguished by the *direct effect of the molecular viscosity* on the turbulent motion. Throughout the flow region, the average Reynolds number varies from one point to the next point. When the flow approaches the wall of the vertical plate, the local turbulent Re decreases. Shuja *et al*. [37] and

Ahmed Abed [38] found that the effects of molecular viscosity are important if the turbulent *Re* is low. Due to this reason, for understanding the nature of the turbulent fluid flow near the plate with a low *Re*, some modifications are necessary. Hence, Jones and Launder [8] suggested that the governing equations hold true and guarantee in the region adjacent to the wall if the LRN k-ε method employs the wall functions (f_1, f_2 and f_μ) and a few more destruction (D) and generation (G) terms. In the vicinity of the wall, the wall function f_μ diminishes the magnitude of time average flow, f_1 amplifies the rate of dissipation and f_2 accounts for the degradation of isotropic turbulence in the LRN region. The values of damping functions used in the current study are based on [12] and are $f_1 = 1$, $f_2 = 1 - 0.3\exp(-Re^2)$ and $f_\mu = \exp\left(\frac{-2.5}{1+\frac{Re}{50}}\right)$. Jones and Launder [8] advised adding a destruction term $D = -2\nu\left(\frac{\partial k^{1/2}}{\partial y}\right)^2$ to the k-equation (Eq. 13) and a generation term $G = 2\nu\nu_t\left(\frac{\partial^2\bar{u}}{\partial y^2}\right)^2$ to the ϵ equation (Eq. 18). The empirical functions used in the LRN k-ε methods were originally designed for *steady* wall bounded turbulent flows, however in the present investigation, these have been extended to *unsteady* turbulent flows.

Therefore, using the above generalization of the k-ε model, the equations for k and ϵ are given below.

$$\frac{\partial k}{\partial t'} + \frac{\partial}{\partial x}(\bar{u}k) + \frac{\partial}{\partial y}(\bar{v}k) = \left(\nu + \frac{\nu_t}{\sigma_k}\right)\frac{\partial^2 k}{\partial y^2} + \nu_t\left(\frac{\partial\bar{u}}{\partial y}\right)^2 - \epsilon - 2\nu\left(\frac{\partial k^{1/2}}{\partial y}\right)^2 \tag{23}$$

$$\frac{\partial \epsilon}{\partial t'} + \frac{\partial}{\partial x}(\bar{u}\epsilon) + \frac{\partial}{\partial y}(\bar{v}\epsilon) = \left(\nu + \frac{\nu_t}{\sigma_\epsilon}\right)\frac{\partial^2 \epsilon}{\partial y^2} + C_1\frac{\epsilon\nu_t f_1}{k}\left(\frac{\partial\bar{u}}{\partial y}\right)^2 - C_2 f_2\frac{\epsilon^2}{k} + 2\nu\nu_t\left(\frac{\partial^2\bar{u}}{\partial y^2}\right)^2 \tag{22}$$

where $\nu_t = C_\mu\frac{k^2}{\epsilon}f_\mu$ denotes the turbulent eddy viscosity.

Now, defining the dimensionless variables listed below:

$$X = Gr^{-1}\frac{x}{l}\ , \quad Y = \frac{y}{l}, \quad U = \frac{Gr^{-1}\bar{u}\,l}{\nu}, \quad V = \frac{\bar{v}l}{\nu}, \quad t = \frac{\nu t'}{l^2}, \quad T = \frac{\bar{T}-\bar{T}_\infty}{\bar{T}_w-\bar{T}_\infty}$$

$$Gr = \frac{g\beta_{\bar{T}}l^3(\bar{T}_w-\bar{T}_\infty)}{\nu^2}\ , \quad K = \frac{kl^2Gr^{-2}}{\nu^2}, \quad E = \frac{\epsilon l^4 Gr^{-2}}{\nu^3}\ , Pr = \frac{\nu}{\alpha_t}\ , \alpha_t = \frac{K_T}{\rho C_p} \tag{23}$$

Introducing Eq. (23) into Eqs. (6)-(8), (19), and (21)-(22), the two-dimensional turbulent free convective dimensionless governing equations are given as follows:

Equation of continuity:

$$\frac{\partial U}{\partial X}+\frac{\partial V}{\partial Y}=0 \tag{24}$$

Equation of momentum:

$$\frac{\partial U}{\partial t}+\frac{\partial}{\partial X}(UU)+\frac{\partial}{\partial Y}(VU)=\left(1+\frac{\nu_t}{\nu}\right)\frac{\partial^2 U}{\partial Y^2}+T \tag{25}$$

Equation of energy:

$$\frac{\partial T}{\partial t}+\frac{\partial}{\partial X}(UT)+\frac{\partial}{\partial Y}(VT)=\left(\frac{1}{Pr}+\frac{\nu_t}{\nu\sigma_T}\right)\frac{\partial^2 T}{\partial Y^2} \tag{26}$$

Equation of kinetic energy:

$$\frac{\partial K}{\partial t}+\frac{\partial}{\partial X}(UK)+\frac{\partial}{\partial Y}(VK)=\left(1+\frac{\nu_t}{\nu\sigma_k}\right)\frac{\partial^2 K}{\partial Y^2}+\frac{\nu_t}{\nu}\left(\frac{\partial U}{\partial Y}\right)^2-E-2\left(\frac{\partial K^{1/2}}{\partial Y}\right)^2 \tag{27}$$

Equation of kinetic energy's dissipation rate:

$$\frac{\partial E}{\partial t}+\frac{\partial}{\partial X}(UE)+\frac{\partial}{\partial Y}(VE)=\left(1+\frac{\nu_t}{\nu\sigma_\epsilon}\right)\frac{\partial^2 E}{\partial Y^2}+C_1\frac{E\nu_t}{\nu K}\left(\frac{\partial U}{\partial Y}\right)^2-C_2[1-0.3\exp(-Re^2)]\frac{E^2}{K}+2\frac{\nu_t}{\nu}\left(\frac{\partial^2 U}{\partial Y^2}\right)^2 \tag{28}$$

where $\frac{\nu_t}{\nu}=C_\mu Re\exp\left(\frac{-2.5}{1+\frac{Re}{50}}\right)$ is the non-dimensional eddy viscosity. The constant values of C_μ, C_1, C_2, σ_T, σ_k and σ_ϵ are given by 0.09, 1.45, 2.0, 0.9, 1.0 and 1.3 respectively.

The following are the dimensionless initial and boundary conditions obtained by substituting dimensionless variables given in Eq. (23) to Eq. (19):

$$\begin{aligned}
&t\le 0 \text{ and } \forall X \,\&\, Y; && U=0,\ V=0,\ K=0,\ E=0,\ T=0\\
&t>0 \text{ and } \text{at } Y=0; && U=0,\ V=0,\ K=0,\ E=0,\ T=1\\
&\text{at } X=0; && U=0,\ V=0,\ K=0,\ E=0,\ T=0\\
&\text{as } Y\to\infty; && U\to 0,\ V\to 0, K\to 0,\ E\to 0,\ T\to 0
\end{aligned} \tag{29}$$

3. Numerical approach:

Transient dimensionless governing (24)-(28) of turbulent flow along with boundary conditions Eq. (29) are solved computationally by using a finite difference approach. Except for unsteady terms, the two-time step level of the Crank-Nicolson scheme is employed for each convective and diffusion terms. Further, the central divided difference scheme is applied to the convective term $\frac{\partial \varphi}{\partial Y}$. Rani *et al.* [40] employed the Crank-Nicolson scheme in their boundary layer study and gave the complete procedure for solving the non-linear coupled partial differential equations in the case of laminar flows. The same procedure can be extended to solve the present investigated coupled non-linear turbulent flow equations. However, the main steps involved in this numerical procedure are given below.

The solutions of Eqs. (24)-(29) are determined in the considered geometry in which $X_{min} = 0$, $X_{max} = 1.0$, $Y_{min} = 0$ and $Y_{max} = 20$. Here Y_{max} is assumed to be away from the average momentum and temperature turbulent boundary layers. The initial mesh size of 100×500 is employed to obtain the numerical values of unsteady time average velocity, energy, turbulent kinetic energy (TKE), and its dissipation rate profiles. These mesh results vary in the second decimal with that of 50×250 and differ in the fifth decimal with 200×100. Thus, for all numerical computations, a mesh (grid) design of 100×500 has been finalized, i.e., with mesh sizes of 0.04 and 0.01 along the Y and X paths, respectively. Additionally, the time dependence's step size has been chosen to be $\Delta t = 0.01$. Further, for unsteady solutions of the average turbulent flow variables, the absolute difference between the flow fields at two successive intervals is smaller than 10^{-5} for all mesh sizes. Initially, the temperature field is obtained by solving the energy Eq. (26). Then velocity U is computed from the Eq. (25) by using known values of T. Similarly, kinetic energy (K) and dissipation rate (E) are also determined from the Eqs. (27) and (28) using the results of Navier-Stokes Eqs. (24) and (25). At the $(n+1)^{\text{th}}$ computation, the finite difference versions of Eqs. (25)-(28) can be represented in the tridiagonal formula, which is given below:

$$A\varphi_{l,m-1}^{n+1} + B\varphi_{l,m}^{n+1} + C\varphi_{l,m+1}^{n+1} = D \tag{30}$$

In the above Eq. (30), symbol φ indicates the dependent variables U, T, K, and E. Consequently, Eq. (30) generates a tridiagonal expression at each inner node on a particular l-level. A Thomas scheme is used to solve these expressions. Also, the velocity, V is calculated directly from Eq. (24) using the obtained values of U. Till to reach the convergence criteria

10^{-5} for all flow field variables, this procedure is repeated for all successive l-levels with longer time steps.

4. Result and discussion:

4.1 Verification of current findings with current solutions:

Lin and Churchill [12] noted that, in the k-ε model ν_t is equated to zero could be used for laminar flows. Accordingly, the comparison results are shown. Hence, the obtained *steady-state simulated time-mean energy and velocity fields of turbulent flow* are compared with the existing laminar results reported by Takhar *et al.* [39]. The present obtained turbulent flow results limited to the laminar case are the same as previous results [39] as shown in Fig. 2 and as well in Table-1, confirming the accuracy of the present approach.

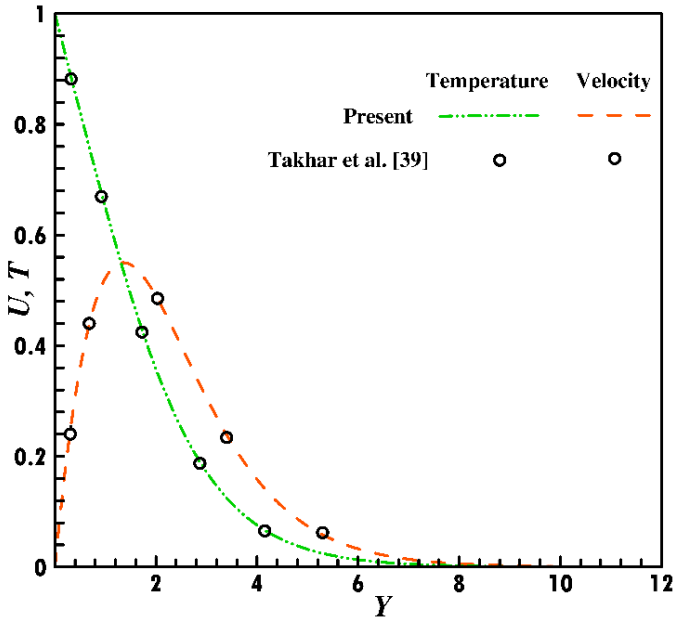

Figure 2: Comparison of the present result with the existing solution of Takhar et al. [39] with fixed $Pr = 0.7$ and $Re = 0.0$.

Pr	Temporal maximum time (t) of		Maximum velocity (U) at $X = 1.0$	$\overline{C_f}$	$\overline{Nu}$
	U	T			
Takhar *et al.* [39]					
0.50	3.90	4.30	0.51	0.80	0.52
0.75	6.04	5.88	0.28	0.65	0.98
1.0	7.13	8.77	0.15	0.44	1.11

Present results: With considering $Re = 0.0$					
0.50	3.90	4.31	0.51	0.8	0.52
0.75	6.05	5.88	0.28	0.65	0.97
1.0	7.13	8.77	0.14	0.44	1.11

Table 1: Validation of present results with Takhar *et al.* [39].

4.2 Analysis of numerical results:

4.2.1 Effect of turbulence Re on turbulent flow fields:

Time-mean velocity field: The simulated time average velocity field U versus t is shown in Fig. 3(a). Initially, it is apparent that all U profiles are merging due to conduction dominating the heat transfer. Further, as time progresses the velocity profile attains its maxima, decreases gradually, and attains asymptotically the steady state. It has been noted that unsteady turbulent flow velocity declines by increasing the Re since the momentum and turbulent kinetic energy production in the flow direction increase as the Re enhances [41]. Figure 3(b) indicates the steady-state turbulent velocity profile with varying values of Re. As noticed from the graph, the initial velocity flow field starts with zero, reaches its maximum values, and decreases monotonically to zero along the Y direction. Further, it has been noted that, as Re raises, the time-independent velocity profile decreases near the hot wall region. However, the same velocity profile shows the reverse trend in the region which is away from the hot surface wall as Re increases. This is due to fact that the effect of turbulent kinetic energy on the velocity field is less near the wall as compared with the turbulence energy dissipation rate. Also, the effect of these two turbulence parameters, k, ε, on the velocity profile produces opposite trends in the region away from the wall.

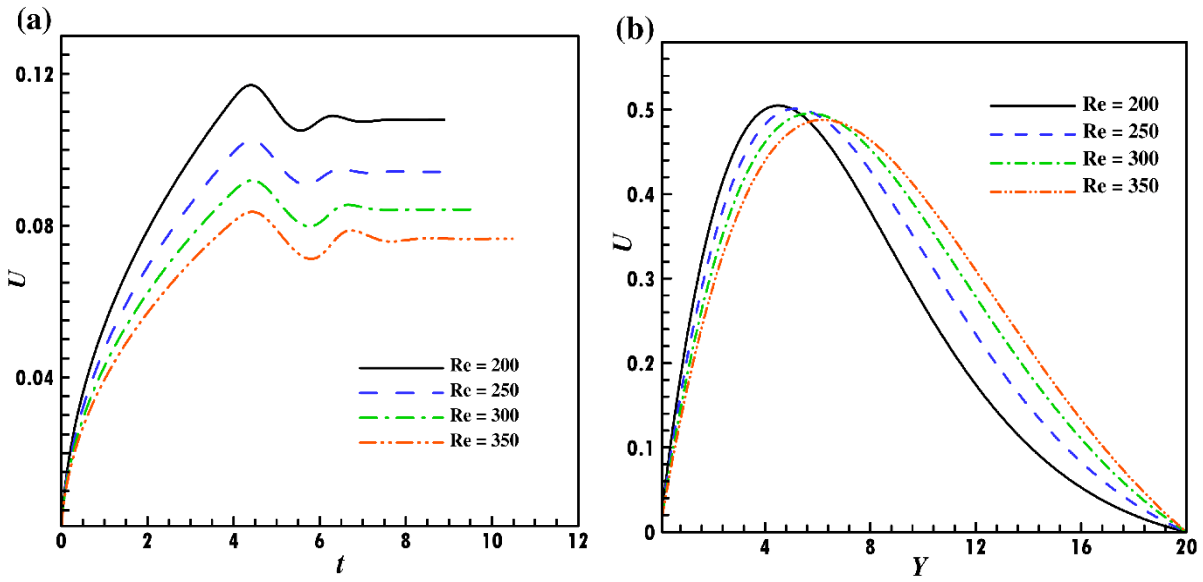

Figure 3: Velocity profiles of the turbulent flow for various values of Re at (a) unsteady state; (b) steady state with fixed $Pr = 0.9$.

Time-mean temperature profile: The unsteady time average temperature field is shown in Fig. 4(a). As noticed from the figure, the temperature field increases as Re increases. Further, the temperature field attains its maxima gradually, shortly thereafter diminishes and again reaches maxima, then decreases, increases, and finally attains the steady state; an oscillatory profile is observed at larger times which is eventually eliminated. Figure 4(b) describes the steady-state time mean temperature profile with altered values of turbulence *Re*. The average energy curves commence at the heated vertical plate at $T = 1$, and decrease monotonically to zero in Ydirection. Also, the steady-state temperature profile increases as Re increased and this trend is sustained throughout the flow domain. However, the same trend is not observed in the velocity profile (Fig. 3(b)).

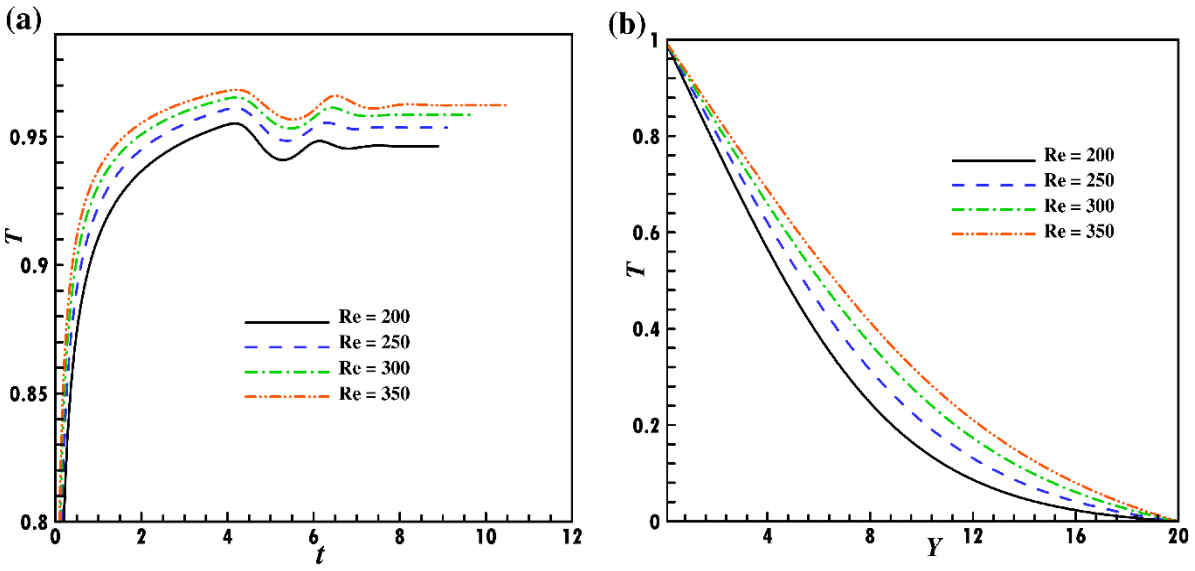

Figure 4: Temperature profiles of the turbulent flow for various values of Re at (a) unsteady state; (b) steady state with fixed $Pr = 0.9$.

Time-mean turbulent kinetic energy (TKE): The unsteady time-mean kinetic energy profile is shown in Fig. 5(a) with varying values of Re. It is noticed that the TKE field increases with time, oscillates finitely, and eventually attains a steady state asymptotically. From Fig. 5(a) it is perceived that the transient nature of the TKE field is not well confirmed for different Re values, however, after reaching the steady state, the TKE field shows significant oscillation. The details about the steady state variation of TKE are depicted in Fig. 5(b). It has been noted that the TKE profile increases drastically in the vicinity of the hot wall and then distributes progressively for varying values of Re. Further, as Re increases, the simulated results of the TKE field increasingly demonstrate a wavy nature with higher amplitude. Since Re is directly proportional to TKE (ref Eq. (20)), therefore the TKE magnitudes increase as Re increases which leads to an increase of velocity in the flow region. Further, these trends are corroborated by earlier studies [41].

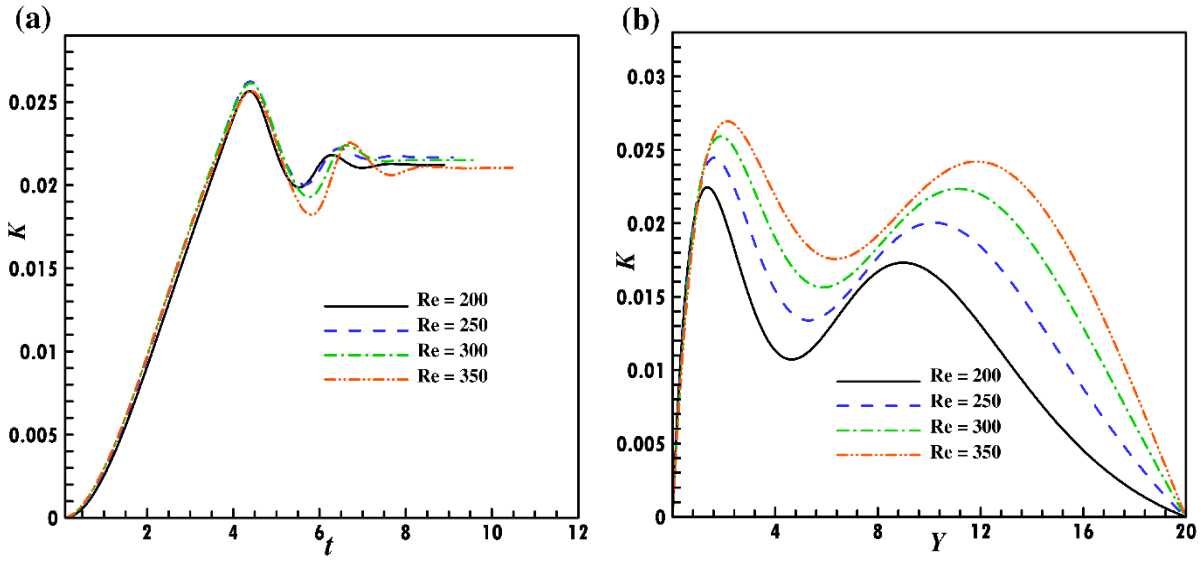

Figure 5: Turbulent kinetic energy profiles for various values of Re at (a) unsteady state; (b) steady state with fixed $Pr = 0.9$.

Time-mean dissipation rate of TKE (turbulence energy dissipation rate): Time-mean simulated transient dissipation rate of the TKE field is portrayed in Fig. 6(a). The dissipation rate of the TKE field declines with the amplifying values of turbulent Re. This is attributable to the enhancing values of Re which decrease the velocity and turbulent production since Re is inversely proportional to the dissipation rate of TKE which is observed in Eq. (20). Initially, the rate of dissipation field increases gradually and reaches its peak value and after slight fluctuation, tends to the *steady state*. Figure 6(b) demonstrates the time average steady state profile of the dissipation rate of TKE at $X = 1$ against Y. Firstly, the rate of dissipation field starts with zero value, progresses slowly and after attaining its peak value, eventually reaches the free stream condition. Also, the dissipation rate field *decreases* until reaches its maxima as an increasing function of Re in the neighborhood of the solid hot plate. However, for the same increasing values of Re a reverse trend is noticed *away* from the wall.

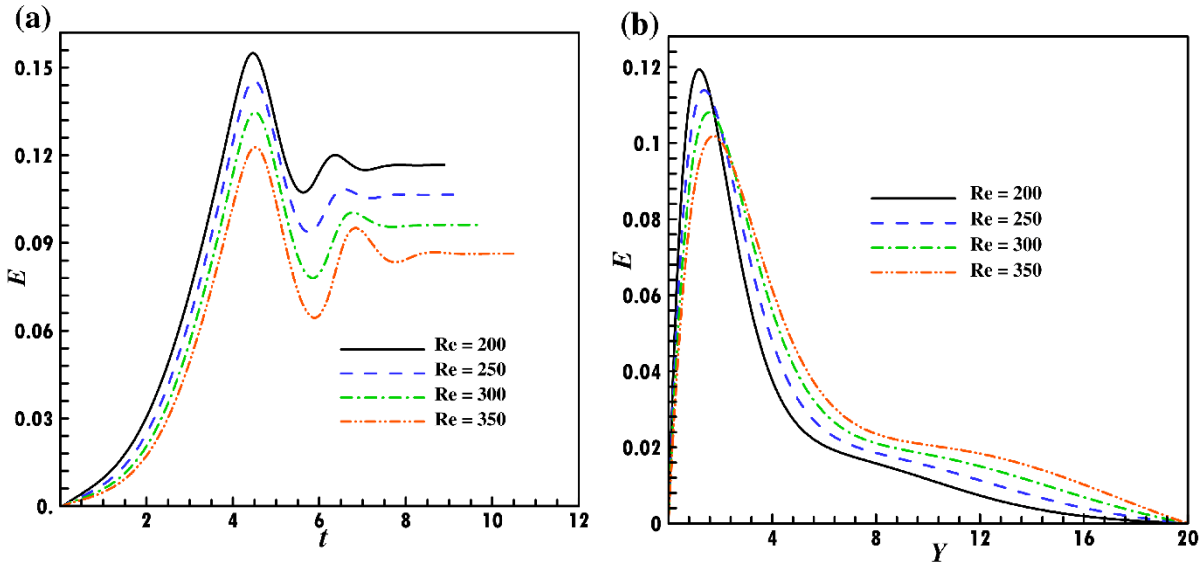

Figure 6: Dissipation rate of TKE profiles for various values of Re at (a) transient state; (b) steady state with fixed $Pr = 0.9$.

4.2.2 Effect of Turbulent Prandtl number (Pr) *on turbulent flow fields.*

Time average velocity field: The simulated time-dependent average velocity field with the effect of Pr is depicted in Fig. 7(a). The transient velocity profiles have a similar turbulent nature as described in Fig. 5(a), i. e. with increasing Pr values, there is a decrease in U profile. It is noted that the average velocity field diminishes with rising Pr since the effect of viscous (momentum) diffusion is amplified for high values of Pr whereas thermal diffusivity is reduced. A similar decreasing trend can be observed in Fig. 7(b) which is drawn against Y. This trend for the effect of Pr on the velocity field for laminar flows has also been reported by Rani *et al.* [40].

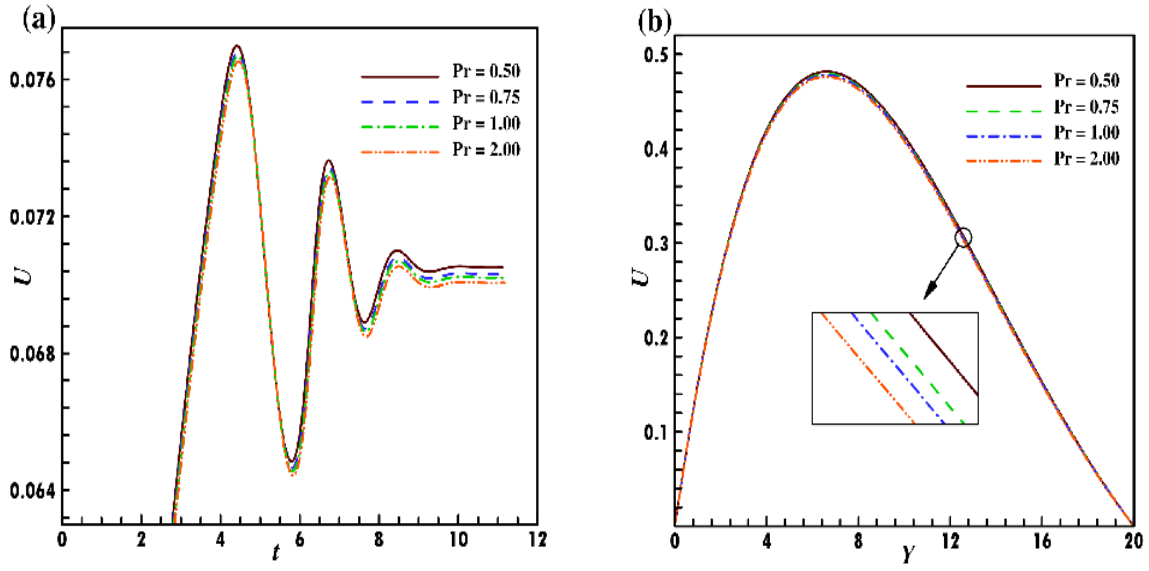

Figure 7: Turbulent velocity profiles for various values of Pr at (a) transient state; (b) steady state with fixed $Re = 400$.

Time average temperature field: Figure 8(a) shows the unsteady simulated time-mean temperature profile for different values of Pr. Initially, with time the temperature profile of turbulent flow is elevated suddenly, attains the maxima and decreases again, then increases and later reaches a steady state. The computed time-mean steady-state temperature profile is shown in Fig. 8(b) at $X = 1$ against Y. The average thermal profile is maximum at the vertical hot plate $(T = 1)\ at\ Y = 0$, and decreases monotonically to zero. Further average temperature profile decreases as Pr increases, since, increasing Pr leads to a decrease in turbulent diffusion terms, resulting in a depletion in heat transfer. This is demonstrated by the definition of turbulent Prandtl number $Pr = \frac{\nu}{\alpha_t}$ (ref Eq. (23)) and further elaborated by Mahdi *et al*. [42].

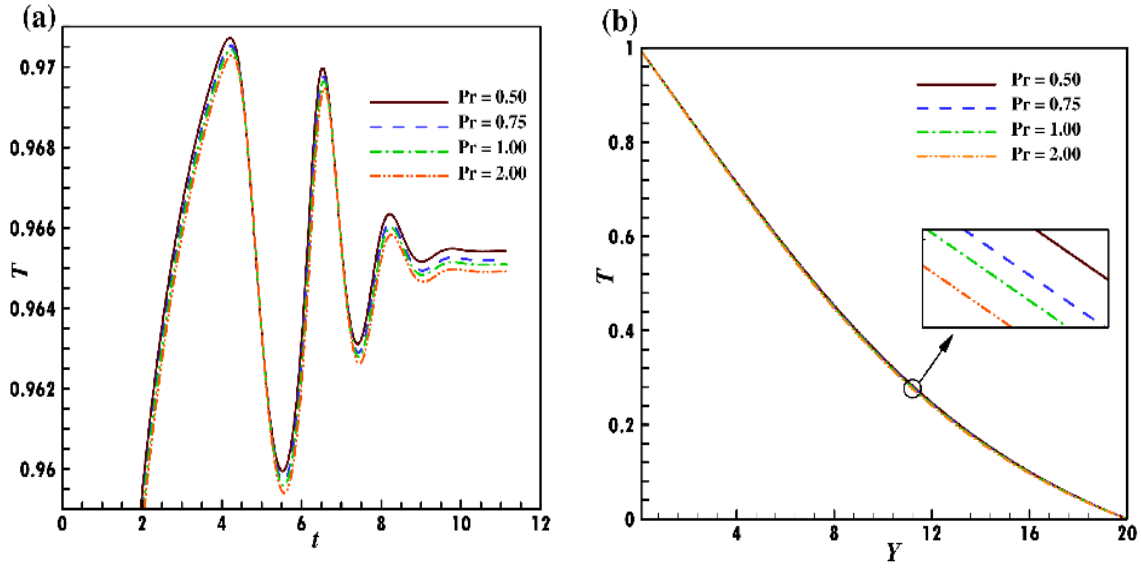

Figure 8: Turbulent temperature profiles for various values of Pr at (a) unsteady state; (b) steady state with fixed $Re = 400$.

Time-average turbulent kinetic energy (TKE): Figure 9(a) discloses computer generated time-average unsteady TKE profile for different trails of Pr. The TKE field reaches its maxima as well as minima smoothly, it repeats up to some time, and then it turns to a steady state. Figure 9(b) shows the simulated time-average steady-state TKE profiles for various values of Pr. These also commence from the origin, attain the maxima and minima, then finally decays to zero. Here also, the TKE profile diminishes as Pr enhances. Since $Pr = \frac{\nu}{\alpha_t}$, which shows that increasing Pr diminishes the thermal diffusion and then retards the growth of TKE [42]. Overall, the steady-state TKE profile shown in Fig. 9(b) is noticed to have a wavy nature for different values of Pr, which is similar to the effect of Re on TKE as shown in Fig. 5(b).

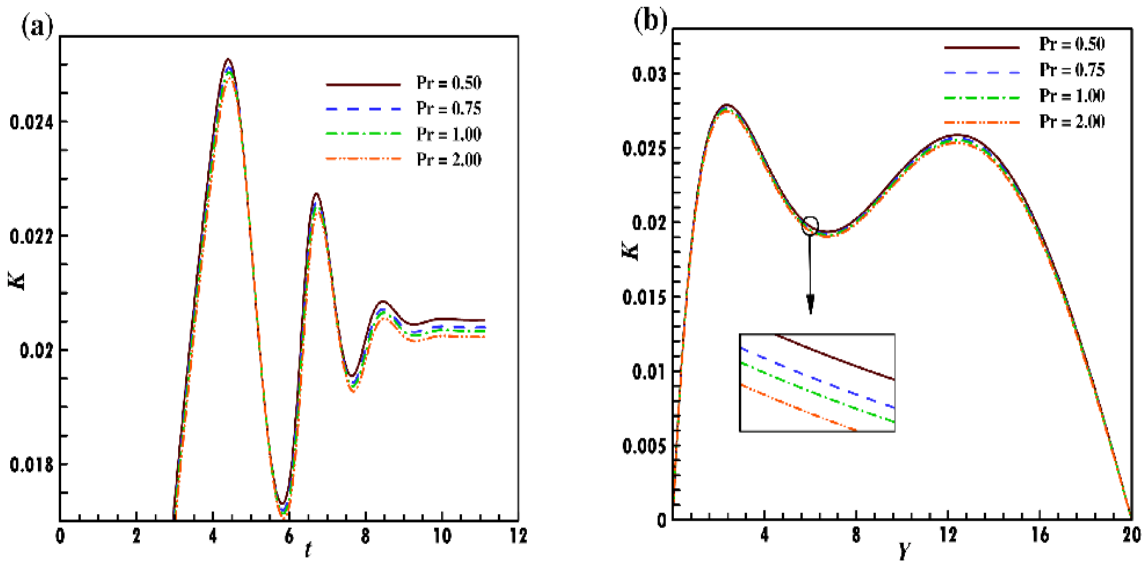

Figure. 9: TKE profiles for various values of Pr at (a) transient state; (b) steady state with fixed $Re = 400$.

Average dissipation rate of TKE: For different values of Pr, the simulated dissipation rate of unsteady time average TKE is shown in Fig. 10(a). The dissipation rate profile originates from the origin, touches the peak value i.e., attains the maxima, and then descends to the minima, later reaching the steady state. Further, at $X = 1$ against Y, the time-mean steady state dissipation rate profile is shown in Fig. 10(b). The steady state dissipation rate profile starts its path from the origin and moves to peak value, later it returns down and gradually reaches zero. Also, from Fig. 10, it is noticed that the dissipation rate profile in both transient and steady state cases decreases with enhancing the values of Pr since increasing Pr retards the thermal diffusion, hence dissipation rate decreased. In both plots, the oscillatory nature of the turbulent flow is captured.

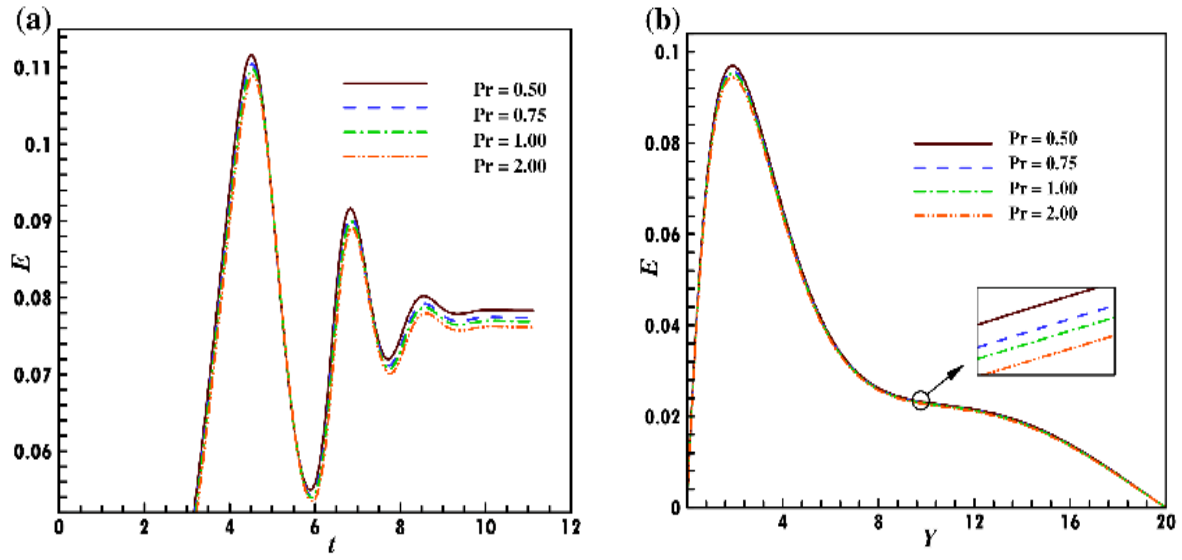

Figure 10: Dissipation rate of TKE profiles for different values of Pr at (a) transient state; (b) steady state with fixed $Re = 400$.

4.3 Average momentum rate $(\overline{C_f})$ and heat transfer rate $(\overline{Nu})$:

Turbulent flow analysis of the average momentum and the heat transfer rate is important from an engineering perspective. The friction factor i.e. the local skin friction coefficient is given below [8]:

$$C_f = \frac{2\tau_w}{\rho \bar{u}_\infty^2} \tag{31}$$

Here τ_w is the total wall shear stress for turbulent flow and is expressed as:

$$\tau_w = \mu \left(\frac{\partial \bar{u}}{\partial y}\right)_{y=0} - \rho \overline{u'v'} \tag{32}$$

Using Eq. (4) and inserting the non-dimensional variables available in Eq. (23), the above Eq. (32) can be expressed in dimensionless form as follows:

$$\tau_w = \frac{\mu Gr(\mu + \mu_t)}{l^2 \rho} \left(\frac{\partial U}{\partial Y}\right)_{Y=0} \tag{33}$$

Rewriting Eq. (31) using Eq. (33) and considering $\frac{2\nu Gr(\nu + \nu_t)}{\bar{u}_\infty^2 l^2}$ be the characteristic of the turbulent shear stress, then the *local turbulent skin friction coefficient* can be written as:

$$C_f = \left(\frac{\partial U}{\partial Y}\right)_{Y=0} \tag{34}$$

The *average turbulent momentum transfer coefficient* can be obtained after the integration of Eq. (34) from $X = 0$ to $X = 1$ along the wall and emerges as:

$$\overline{C_f} = \int_0^1 \left(\frac{\partial U}{\partial Y}\right)_{Y=0} dX \tag{35}$$

The *local turbulent heat transfer rate* is calculated as follows:

$$Nu = \frac{l q_w}{(\bar{T}_w - \bar{T}_\infty) K_T} \tag{36}$$

Here, local energy-flux density, q_w is given by $q_w = -K_T \left(\frac{\partial \bar{T}}{\partial y}\right)_{y=0} = -K_T \frac{\bar{T}_w - \bar{T}_\infty}{l} \left(\frac{\partial T}{\partial Y}\right)_{Y=0}$.

Thus, using the non-dimensional variables given in Eq. (23), the *turbulent local Nusselt number* using Eq. (36), can be written as:

$$Nu = -\left(\frac{\partial T}{\partial Y}\right)_{Y=0} \tag{37}$$

Integration of Eq. (37) from $X = 0$ to $X = 1$ along the wall gives the following *average turbulent Nusselt number* (energy transfer rate):

$$\overline{Nu} = -\int_0^1 \left(\frac{\partial T}{\partial Y}\right)_{Y=0} dX \tag{38}$$

The above Eqs. (35) and (38) are evaluated through the approximated five-point formula and later, the integrals are computed by utilizing a Newton-Cotes integration scheme.

4.3.1 Effect of Re on turbulent average momentum $(\overline{C_f})$ and heat transfer $(\overline{Nu})$ rates:

Figure 11 illustrates the variation of the average friction parameters for various values of Re. The simulated average skin-friction coefficient of the turbulent flow profile on Re has been plotted against time t and is displayed in Fig. 11(a). It is observed that, $\overline{C_f}$ augmented with time, attains its peak value, and becomes asymptotically steady. Also skin friction coefficient is observed to attain the *steady state* with time increasing for the first ($Re = 200, 250$) and last ($Re = 300, 350$) two values. It is also noticed that the $\overline{C_f}$ reduces for enhancing the values of Re. This is due to the fact that with the increase of Re, the interaction between the shear stress and flow speed changes, and the same result is noted in [41]. The simulated $\overline{Nu}$ for turbulent flow has been drawn in Fig. 11(b) against t with the impact of Re. It reveals that the turbulent heat transfer decreases for increasing values of Re since it is directly connected to the formula $\overline{Nu}$ with a negative sign of temperature profile (Eq. (38)). Therefore, the average energy profile plotted in Fig. 4 is in line with this result. The heat transfer rate field is high at the initial time near the plate, later decreases and eventually tends to a steady state.

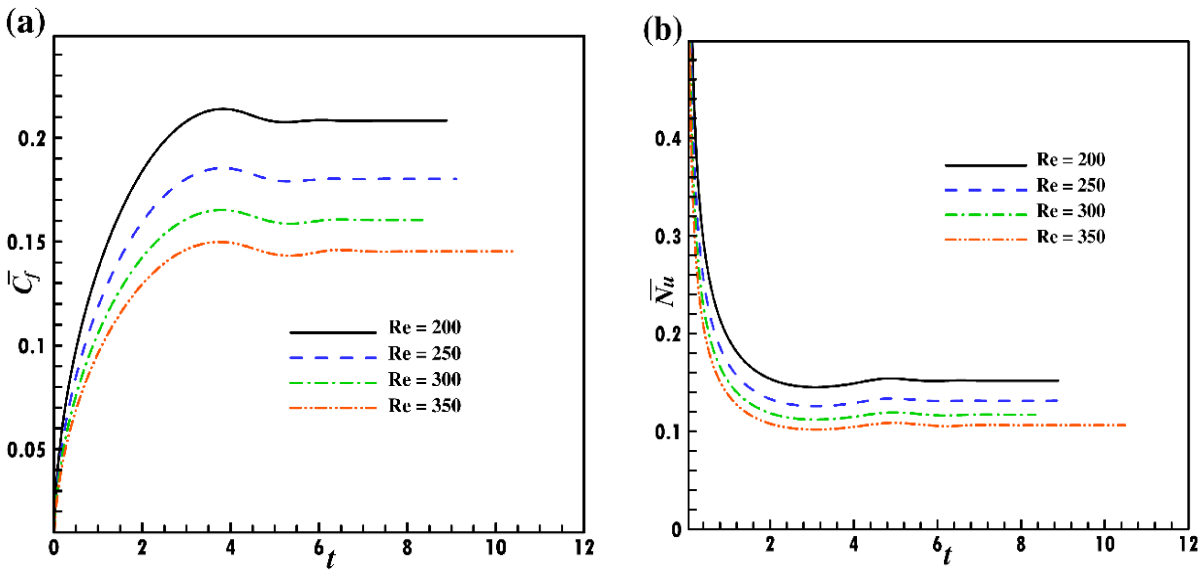

Figure 11: (a) Average surface friction coefficient, $\overline{C_f}$; (b) turbulent heat transfer rate, $\overline{Nu}$ profiles for different values of Re with fixed $Pr = 0.9$.

4.3.2 Effect of Pr on $\overline{C_f}$ and $\overline{Nu}$:

Figure 12 depicts the average friction factors for various values of Pr. The simulated average surface-friction coefficient of turbulent flow relating to Pr has been plotted against time t and is presented in the Fig. 12(a). It is observed that, $\overline{C_f}$ is augmented with time, attains its maxima, as well as minima, and continues to ascend in magnitude until it becomes asymptotically steady. It is also noticed that the $\overline{C_f}$ diminishes for amplifying values of Pr, since Pr is the ratio of viscosity to thermal diffusion, hence increasing Pr enhances the viscosity, which leads to diminishes the skin friction coefficient. Also, this result is consistent with the average velocity profiles plotted in Fig. 7 which are directly connected to the formula $\overline{C_f}$ which involves the velocity profile (Eq. (35)). Further, the simulated $\overline{Nu}$ has been drawn against t with the impact of Pr as shown in Fig. 12(b). It is evident that the $\overline{Nu}$ values i. e. heat transfer rates at the plate, increase for increasing values of Pr. This is because an increase in Pr leads to the rate of heat transmission being intensified by the *spatial decay* of the temperature field near the heated surface, which effectively yields an increase in the $\overline{Nu}$.

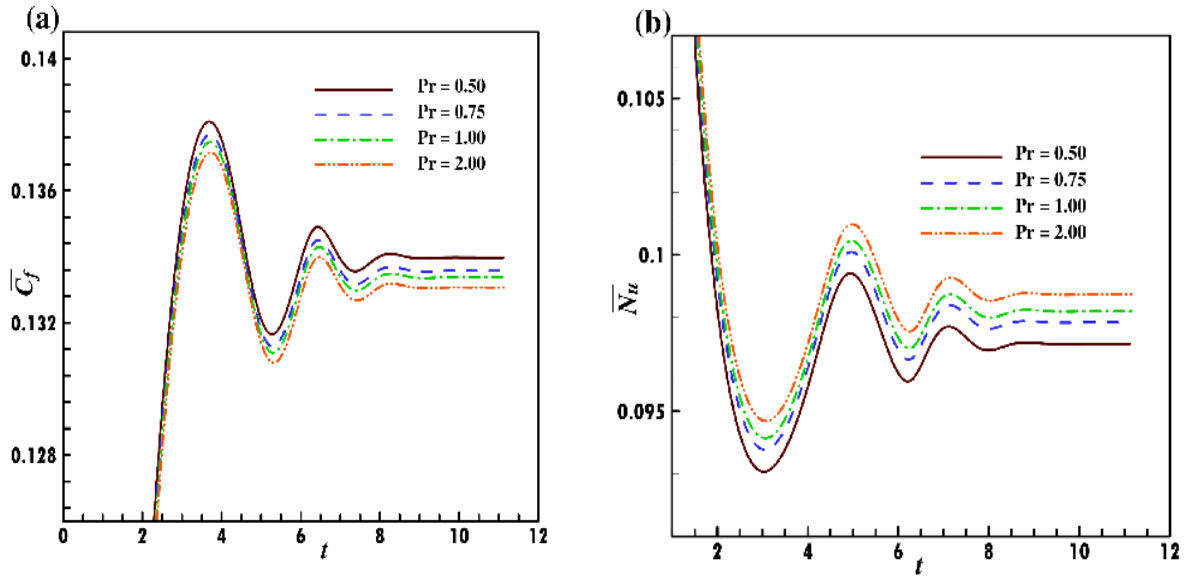

Figure 12: (a) Average surface friction coefficient, $\overline{C_f}$; (b) heat transfer rate turbulent profiles, $\overline{Nu}$ for various values of Pr with fixed $Re = 400$.

5. Conclusions:

In this article, a numerical study of transient buoyancy-driven turbulent boundary layer flow from a semi-infinite vertical plate with the help of the LRN two-equation *k*-ε turbulence method has been presented. The governing turbulent flow-field equations have been solved with associated boundary conditions using a robust implicit finite difference Crank-Nicholson scheme. The numerical results have been displayed graphically and analyzed in terms of velocity, temperature, turbulent kinetic energy, dissipation rate, and friction factors for different values of turbulence low Reynolds (Re) and Prandtl (Pr) numbers. From the present turbulent flow analysis, the following conclusions can be made.

- The solutions of transport equations for turbulent kinetic energy and its dissipation rate are used to estimate the local value of turbulent viscosity, ν_t.
- The average transient velocity and turbulence energy rate profiles decrease, and the temperature profile increases by increasing Re values.
- The average steady temperature and turbulence energy profiles increase with increment in values of Re.
- The average velocity, temperature, turbulence energy, and dissipation rate under both transient and steady state conditions decrease with amplifying values of Pr.
- The average turbulent momentum and the heat transfer rates are decreased by increasing Re values.

- The average turbulent momentum is reduced and the average Nusselt number (wall heat transfer rate) is elevated with rising Pr values.

The LRN two-equation k-ε turbulence method and implicit Crank Nicholson finite difference numerical approach has been shown to yield physically viable results for two-dimensional turbulent buoyancy-driven convection boundary layer flows. The present research work on Newtonian turbulent boundary layer flows may be further extended to non-Newtonian fluids with different physical and chemical effects for various geometries [44-49]. Also, it is envisaged that the current study may be broadened to explore the application of the LRN turbulence modeling approach to other areas of engineering sciences such as chemical engineering, coating flows, etc. Additionally, the present simulations are also of interest in micromixing techniques which occur at small time scales as predicted by the TKE and its dissipation rate which has been noted by Guichao *et al.* [50]. Furthermore, turbulent natural convection flows constitute one of the most fundamental topics in engineering fluid dynamics. Such flows feature in meteorology via atmospheric circulation induced by solar radiation. The present computations may also be relevant to other areas including the refrigeration of electronic components [51], ventilation of rooms, cooling of electronic devices, and airflow in buildings to reduce noise exposure [52], wedge-induced oblique detonations [53] and optimization of ducted propeller hovering performance [54]. Efforts in these areas consotute a rich pathway for future implementation of the present numerical approach.

Acknowledgments:

The authors wish to express their gratitude to the reviewers who highlighted important areas for improvement in the earlier draft of this article. Their suggestions have served specifically to enhance the clarity and depth of the interpretation of results in the revised manuscript.

References:

1. Mahdi, M. A., Smaili, A., and Saad, Y., Numerical investigations of turbulent natural convection heat transfer within a wind turbine nacelle operating in hot climate, *International journal of thermal sciences*, 147, 106-143 (2020).
2. Tabrizi, A. B. and Jaluria, Y., Application of steady-state turbulent flow data in the solution of inverse natural heat convection problems, *International journal of heat and mass transfer*, 164, 120553 (2020).

3. Miroshnichenko, I. V., and Sheremet, M. A., Turbulent natural convection heat transfer in rectangular enclosures using experimental and numerical approaches: A review, *Renewable and sustainable energy reviews*, 82, 40-59 (2018).
4. Tkachenko, S., Timchenko, V., Yeoh, G., and Reizes, J., Effects of radiation on turbulent natural convection in channel flows. *International journal of heat and fluid flow*, 77, 122-133 (2019).
5. Warner, C. Y., and V. S. Arnaci, V. S., An experimental investigation of turbulent natural convection in air at low pressure along a vertical heated that plate. *International Journal of heat and mass transfer*, 11, 397-406 (1968).
6. Pirovano, A., and Jannot, S.V.M., Convection naturelle En regime turbulent Le long d'une plaque plane verticale, *Proceeding 9th international heat transfer conference; Natural convection*, 4, 1- 12 (1970).
7. Smith, R. R., Characteristics of turbulence in free convection flow past a vertical plate, *Ph.D. Thesis, University of London* (1972).
8. Jones, W. P., and Launder, B. E., The prediction of laminarization with a two-equation model of turbulence, *International journal of heat and mass transfer*, 15, 301-314 (1972).
9. Jones, W. P., and Launder, B. E., The calculation of low Reynolds number phenomena with a two-equation model of turbulence, *International journal of heat and mass transfer*, 16, 1119-1130 (1973).
10. Mason, H. B., and Seban, A. R., Numerical predictions for turbulent free convection from vertical surfaces, *International journal of heat and mass transfer*, 77, 1329-1336 (1974).
11. George, W. K., and Capp, S. P., A theory for natural convection turbulent boundary layers next to heated vertical surfaces, *International journal of heat and mass transfer*, 22, 813-826 (1978).
12. Lin, S. J., and Churchill, S. W., Turbulent free convection from a vertical isothermal plate, *Numerical heat transfer, Part B: Fundamentals*, 1,129-145 (1978).
13. Chien, K. Y., Predictions of channel and boundary layer flows with a low Reynolds number turbulence model, *American institute of aeronautics and astronautics journal*, 20, 33-38 (1982).
14. Patel, V. C., Turbulence models for near-wall and low Reynolds number flows: A Review, *American institute of aeronautics and astronautics journal*, 23, 1308-1319 (1985).

15. Jalal M. Jalil, Talib K. Murtadha, and Kays A., Al-Taey, Laminar and turbulent natural convection heat transfer of a liquid metal in an enclosed enclosure, *Engineering journal of the University of Qatar*, 19, 2006.
16. Fedorov, A. G., Viskanta, R., and Mohamud, A. A., Turbulent heat and mass transfer in an asymmetrically heated vertically parallel channel, *International journal of heat and fluid flow*, 18, 307-315 (1997).
17. Atila, A. I., and Mehmet E. A., A comparative study of four Low-Reynolds-number k-ε turbulence models for periodic fully developed duct flow and heat transfer, *Numerical heat transfer, Part B: Fundamentals*, 69, 234-248 (2016).
18. Kuzmin, D., Mierka, O., and Turek, S., On the implementation of the k-ε turbulence model in incompressible flow solvers based on a finite element discretization, *International journal computing science and mathematics*, 1, 1-9 (2007).
19. Fedorovich, E., and Shapiro, A., Turbulent natural convection along a vertical plate immersed in a stably stratified fluid, *Journal of fluid mechanics*, 636, 41-57 (2009).
20. Rathore, S.K., and Das, M. K., Comparison of two low Reynolds number turbulence models for fluid flow study of wall bounded jets, *International journal of heat mass transfer*, 61, 365-380 (2013).
21. Rath, S., and Dash, S. K., Numerical study of laminar and turbulent natural convection from a stack of solid horizontal cylinders, *International Journal of thermal sciences*, 106-147 (2019).
22. Acharya, S., and Dash, S. K., Turbulent natural convection heat transfer from a vertical hollow cylinder suspended in air: A numerical approach, *Thermal science and engineering progress*, 15, 1-36 (2019).
23. Cousteix, J., and Houdeville, R., Effects of unsteadiness on turbulent boundary layers, *von Karman institute for fluid dynamics: Lecturer series*, 93, 6-34 (1983).
24. Justesen, P., and Spalart, P. R., Two-Equation turbulence modelling of oscillatory boundary layers, *AIAA 28TH Aerospace sciences meeting, Reno, Nevada, January*, 10, 1-14 (1990).
25. Mankbadi, R. R., and Mobark, R., Quasi-steady turbulence modelling of unsteady flows, *International journal of heat and fluid flow*, 12, 122-129 (1991).
26. Fan, S., Lakshminarayana, B., and Barnett, M., Low Reynolds number k-ε model for unsteady turbulent boundary layer flows, *American institute of aeronautics and astronautics journal*, 31, 1777-1784 (1993).

27. Abe, K., Kondoh, T., and Nagano, Y., A new turbulence model for predicting fluid flow and heat transfer in separating and reattaching flows-II; Thermal field calculations, *International journal of heat and mass transfer,* 38, 1467-1481 (1995).
28. Bredberg J., and Davidson, L., Low Reynolds number turbulence model; An approach for reducing mesh sensitivity, *ASME Journal of fluids engineering,* 126,14-21 (2004).
29. Bentaleb, Y., Schall, E., and Kousksou, T., Numerical prediction of wall-bounded flows with Low-Reynolds k-ε turbulence models, *Progress in computational fluid dynamics,* 9, 96-108 (2009).
30. Nie, X., and Li, L., A Comparison of low Reynolds number k-ε models, 4th *International conference on Computer, Mechatronics, Control and Electronic engineering, Hangzhou, China ,* 1334-1339 (2015).
31. Behera, V. M., and Rathore, S. K., Numerical study on turbulent characteristics of wall jet in a quiescent environment over a plate in motion, *IOP Conference series: Materials science and engineering, Gandhinagar, India, March* (2021).
32. Wen, X., Wang, L. P., Zhaoli, G., and Zhakebayev, D. B., Laminar to turbulent flow transition inside the boundary layer adjacent to isothermal wall of natural convection flow in a cubical cavity, *International journal of heat and mass transfer,* 167, 1-19 (2021).
33. Rathore, S. K., Study of conjugate heat transfer from heated plate by turbulent offset jet in presence of freestream motion using Low-Reynolds number modelling, *Journal of applied fluid mechanics,* 12, 617-630 (2019).
34. Rosti, E. R., and Brandt, L., Low Reynolds number turbulent flows over elastic walls, *Physics of Fluids*, 32, 1-10 (2020).
35. Mahammedi, A., Ameur, H., Menni, Y., and Medjahed, D. M., Numerical study of turbulent flows and convective heat transfer of Al_2O_3-water Nanofluids in a circular tube, *Journal of advanced research in fluid mechanics and thermal sciences*, 77, 1-12 (2020).
36. Behera, V. M., and Rathore, S. K., Numerical investigation of turbulent offset jet flow over a moving flat plate using low-Reynolds number turbulence model, *ASME Journal of thermal science and engineering applications,* 13, 1-32 (2021).
37. Shuja, S. Z., Yilbas, B. S., and Budair, M. O., Gas jet impingement on a surface having a limited constant heat flux area: various turbulence models, *Numerical heat transfer,* 36,171- 200 (1999).

38. Ahmed Abed Majhool., Effect of turbulent Prandtl number in the convective turbulent heat transfer modelling, *Al-Qadissiya journal of engineering*, 7, 306-321 (2014).
39. Takhar, H.S., Ganesan, P., and Ekambavanan, K., Transient free convection past a semi-infinite vertical plate with variable surface temperature**,** *International journal of numerical methods for heat and fluid flow,* 7, 280-296 (1997).
40. Rani, H. P., Reddy, G. J., and C. N. Kim., Numerical analysis of couple stress fluid past an infinite vertical cylinder, *Engineering applications of computational fluid mechanics,* 5, 159-169 (2011).
41. Farhad, V., and Mohadeseh, M., Numerical study of the effect of the Reynolds numbers on thermal and hydrodynamic parameters of turbulent flow mixed convection heat transfer in an inclined tube, *Journal of Mechanical Engineering,* 61, 669-679 (2015).
42. Mahdi, M., and Majid, B., Effect of turbulent Prandtl number on convective heat transfer to turbulent flow of a supercritical fluid in a vertical round tube, *ASME Journal of heat transfer,* 133, 1-10 (2011).
43. To, W. M., and Humphrey, J. A. C., Numerical simulation of buoyant, turbulent flow-I, Free convection along a heated vertical flat plate, *International journal of heat and mass transfer,* 29, 573-592 (1986).
44. Metzner, A.B.; Reed, J.C. Flow of non-Newtonian fluids-Correlation of the laminar, transition and turbulent-flow regions. *American institute of chemical Engineers,*1, 434-440 (1955).
45. Machireddy, G. R., Praveena, M.M., Rudraswamy, N. G., and Kumar, G. K., Impact of Cattaneo–Christov heat flux on hydromagnetic flow of non-Newtonian fluids filled with Darcy–Forchheimer porous medium, *Waves in random and complex media,* 2021.
46. Ravi, R., Kanchana, C., Reddy, G. J., and Basha, H., Study of Soret and Dufour effects and secondary instabilities on Rayleigh-Benard convection in a couple stress fluid, *The European physical journal plus,* 133, 1-14 (2018).
47. Srinivasa, J., Anwar Beg, O., Homotopy study of entropy generation in magnetized micropolar flow in a vertical parallel plate channel with buoyancy effect, *Heat transfer research*, 49, 529-553 (2018).
48. Ashwini Hiremath, G. Janardhana Reddy, O. Anwar Bég & Harish Holla (2022), Numerical investigation on transient third-grade magnetized nanofluid flow and radiative convection heat transfer from a stationary/moving cylinder: nanomaterial and nanoparticle shape effects, *Waves in Random and Complex Media*, DOI: 10.1080/17455030.2021.2024300.

49. Bhaskerreddy Kethireddy, G. Janardhana Reddy & Hussain Basha (2022), Bejan's thermal and mass flow visualization in micropolar fluid, *Waves in Random and Complex Media*, DOI: 10.1080/17455030.2022.2088887.
50. Guichao, W., Fan, Yang., Ke Wu., Yongfeng Ma., Cheng Peng., Tianshu Liu., and Lian-Ping, W., Estimation of the dissipation rate of turbulent kinetic energy: A review, *Chemical Engineering Science*, 229, 1-17 (2021).
51. Rincon-Casado, A., Sanchez de la Flor, F. J., Chacon Vera, E., and Sanchez Ramos, J., New natural convection heat transfer correlations in enclosures for building performance simulation, *Engineering applications of Computational Fluid Mechanics*, 1,340-356 (2017).
52. Zimmermann, Claudia, and Rodion, G., Modelling turbulent heat transfer in a natural convection flow**,** *Journal of Applied Mathematics and Physics*, 2, 662-670 (2014).
53. Pengfei, Yang, Hoi Dick Ng and Honghui, T., Numerical study of wedge-induced oblique detonations in unsteady flow, *Journal of Fluid Mechanics*, 876, 264-87(2019).
54. Hu Yu, Ji xiang Qing, Zhong, H. L., Zachary, J. C., Jia Ning Cao, and Xue Peng Zhang, Hovering efficiency optimization of the ducted propeller with weight penalty taken into account, *Aerospace Science and Technology*, 117, 106937(2021).